Journal of Materials, Processing and Design (2024)
Clausius Scientific Press, Canada

DOI: 10.23977/jmpd.2024.080210
ISSN 2516-0923 Vol. 8 Num. 2

Effect of anodization time on the properties of rGO doped titanium oxide films

Di Shan*, Huan Yang, Hui Shao, Changqing Fang, Yuzhen Wang, Wei Shi, Kun Wang

Xi'an University of Technology, Xi'an, 710048, China
**Corresponding author: shandigood@163.com*

Keywords: Titanium, Anodizing, Chemical composition, Corrosion resistance

Abstract: The pure titanium was anodized in reduced graphene oxide (rGO) / citric acid (C6H8O7) aqueous electrolyte at 50 V. Six samples were taken within 60 min based on the current-time relationship to investigate the microstructure, phase composition, hardness, and corrosion resistance. The results revealed that in the initial 2 min, the oxide film in the growth stage showed a noticeable increase in thickness. The film consisted of various non-steady state oxides such as Ti3O5 and Ti2O3. Subsequently, from 2 to 9 min, the oxide film is in the dissolution stage, characterized by a high content of lattice O^{2-}, high crystallinity and low structural defects. The nano-hardness and corrosion resistance of the oxide film in this stage were superior to those of other samples. Finally, from 9 to 60 min, the oxide film continued to grow slowly towards a balanced stage. The oxide film thickness increased slightly, while the lattice O^{2-} content decreased and structural defects increased, resulting in decreased hardness and corrosion resistance. Therefore, it is recommended to maintain the oxidation time between 5 to 9 min during the dissolution stage to achieve a high-performance oxide film.

1. Introduction

Titanium oxides consist of various proportions of Ti and O atoms, such as Ti2O, TiO, Ti2O3, Ti3O5, TiO2 [1-2]. Among these, TiO2 is the stable phase of titanium oxides. In the natural environment, nano-scale amorphous TiO2 forms on the surface of titanium, which can provide a certain degree of protection to the substrate, but with limited mechanical properties and corrosion resistance. Surface modifications such as electroplating, electrophoretic deposition, micro-arc oxidation and anodic oxidation [3~6] are commonly used. Anodic oxidation, in particular, offers good controllability, simple operation, and uniform film formation, making it widely utilized in titanium surface modification.

The performance of anodic oxide film is closely related to the type of electrolyte, oxidation potential and oxidation time [7~9]. Currently, anodic oxidation of titanium is usually carried out in environmentally unfriendly electrolytes containing strong acids, strong bases, or electrolytes with fluorine ions [10~11]. These electrolytes are highly volatile and can pose health risks to operators even in well-ventilated environments. In addition, anode oxidation in these electrolytes results in the continuous dissolution of Ti^{4+} into the solution. It is necessary to update the electrolyte regularly and recycle the waste chemical solution safely. In this paper, the electrolyte used is a solution of C6H8O7

and rGO electrolyte. The rGO is non-toxic and can be recycled easily. C6H8O7 is an additive commonly found in food and cosmetics. The solvent used is water. All components in the electrolyte are environment friendly, eliminating the need to consider issues related to the working environment and waste solution recovery.

Previous research has conducted anodic oxidation of pure titanium in rGO/C6H8O7 aqueous electrolyte in the voltage range of 0 ~ 90 V. When the voltage is 50 V, the oxidation film exhibits high crystallinity and density, as well as excellent corrosion resistance [12]. In this study, the effects of oxidation time on the microstructure, chemical composition, nano-hardness and corrosion resistance of the oxide film have been studied by varying the oxidation time from 0 to 60 min at a constant voltage of 50 V.

2. Materials and experimental procedures

2.1 Materials and pretreatment

The chemical composition (wt%) of pure titanium used in anodization was 0.061% Fe, 0.0028% C, 0.002% H, 0.006% N, 0.087% O and 99.816% Ti. The sample dimensions were 30 × 50 × 3 mm³. The sample surface was polished with Al2O3 paper ranging from 400 to 2000 grit to achieve a smooth surface. All samples were ultrasonically cleaned in an ethanol solution, followed by rinsing in deionized water, and drying in an air stream.

2.2 Anodization

The samples were subjected to anodic oxidation in an electrolyzer equipped with a magnetic stirrer using a standard two-electrode system. The Ti sample served as the anode, while a Pt plate was used as the cathode. The distance between anode and cathode was 6 cm. The preparation process of the rGO/C6H8O7 aqueous electrolytes can be found in the paper [12]. The stirring speed during the treatment was 100 r/min, and the electrolyte temperature was maintained at 25 ± 2°C. Anodization treatment was carried out at 50 V for different durations ranging from 0 to 60 min. A precision ammeter connected to a computer terminal recorded the current changes over time. After multiple experiments, the error in the current-time relationship was controlled within ± 0.1 s. Six specific time points were identified within 60 min based on the current-time relationship, at 0.005, 2, 5, 9, 30, and 60 min respectively. The corresponding samples were labeled as Ti-0.005, Ti-2, Ti-5, Ti-9, Ti-30, and Ti-60.

2.3 Performance characterization

The surface morphology and coating thickness were observed by Scanning electron microscope (SEM). The phase composition and crystallinity of the samples were analyzed by Raman spectroscopy. X-ray photoelectron spectroscopy (XPS) was used to analyze the element types and atomic contents of the samples. The hardness and elastic modulus of the oxide film were obtained by measuring the average values of five indentations with a nano-indentation instrument under a maximum pressure of 2000 μN. Electrochemical analysis of the samples was performed in a 3.5 wt% NaCl solution using the CHI660E electrochemical workstation. The apparatus was composed of a standard two-chamber electrolysis cell with three electrodes: a working electrode, a platinum auxiliary electrode and a saturated calomel reference electrode. The electrolysis cell was controlled by a potentiostat. The open circuit potential-time curve (*E*ocp-*t*) was recorded. The Tafel polarization curve was achieved at a scan rate of 1 mV/s from *E*ocp -350 mV to *E*ocp +350 mV.

3. Results and discussion

3.1 Growth process of oxide film

At a constant voltage of 50 V, the current-time curve is shown in Fig. 1. From 0 to 2 min, it is identified as stage (I), during which the current rapidly decreased from its peak value, indicating the initial growth stage of the oxide film. Between 2 and 9 min, labeled stage (II), the current showed an upward trend. During the stage, the dissolution rate of the oxide film exceeded the growth rate. From 9 to 60 min, marked as stage (III), the current gradually decreased and stabilized, while the oxide film grew slowly and tended to balance. The color of the oxide film changed from dark brown to yellow and then to light brown.

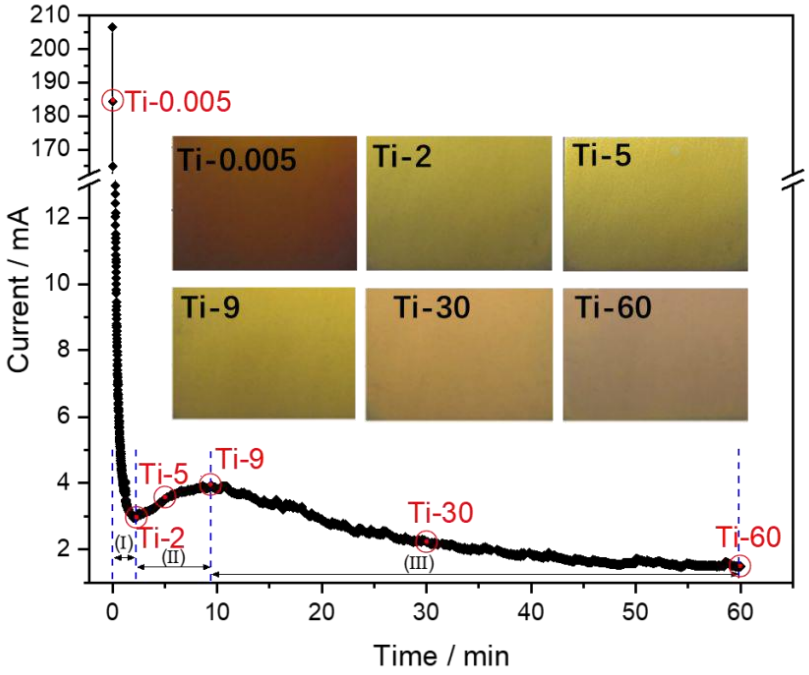

Figure 1: Current-time curve of the samples anodized at 50 V

3.2 Microstructural characterization

Fig. 2 shows the microstructure of the oxide film anodized at different times. As the oxidation time increases, the scratches made by sandpaper are shallower, indicating thickening of the oxide film. During stage (I), there was a high growth rate of the oxide film upon connecting the power supply. The oxide film is pore-free. The thickness of the oxide film was measured using SEM technology, and multiple measurements revealed that the thickness of Ti-0.005 is 6.3 ± 0.2 μm. In stages (II) and (III), the rate of thickening of the oxide film obviously slows down. When the oxidation time reaches 60 min, the thickness of Ti-60 is 7.3 ± 0.2 μm. The primary thickening of the oxide film occurs in stage (I) compared to other stages. The presence of black spots on the Ti-60 surface suggests localized breakdown, leading to higher structural defects in Ti-60 compared to other samples.

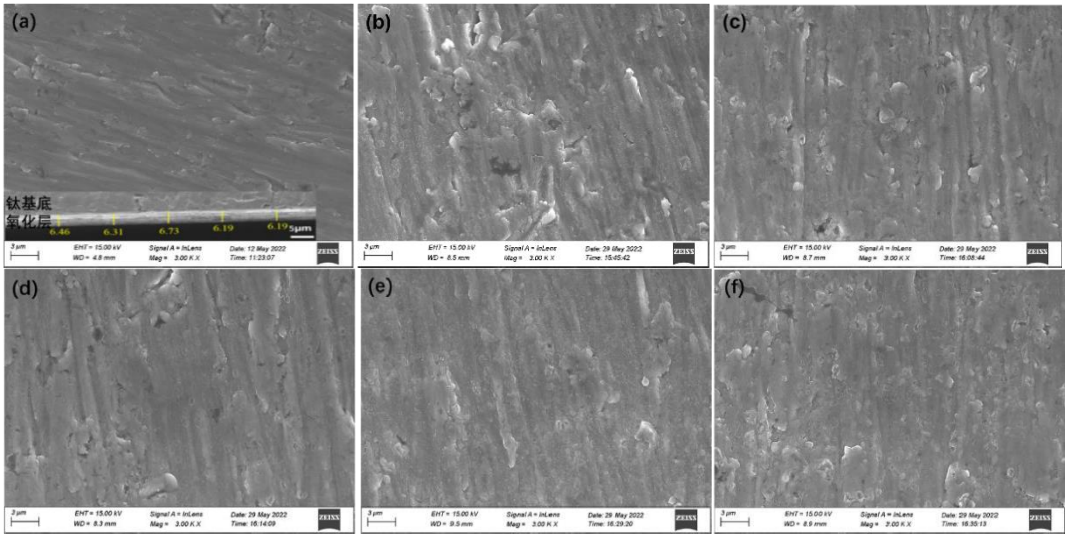

(a)Ti-0.005, (b) Ti-2, (c) Ti-5, (d) Ti-9, (e) Ti-30 and (f) Ti-60

Figure 2: SEM images of the oxide films anodized at different times:

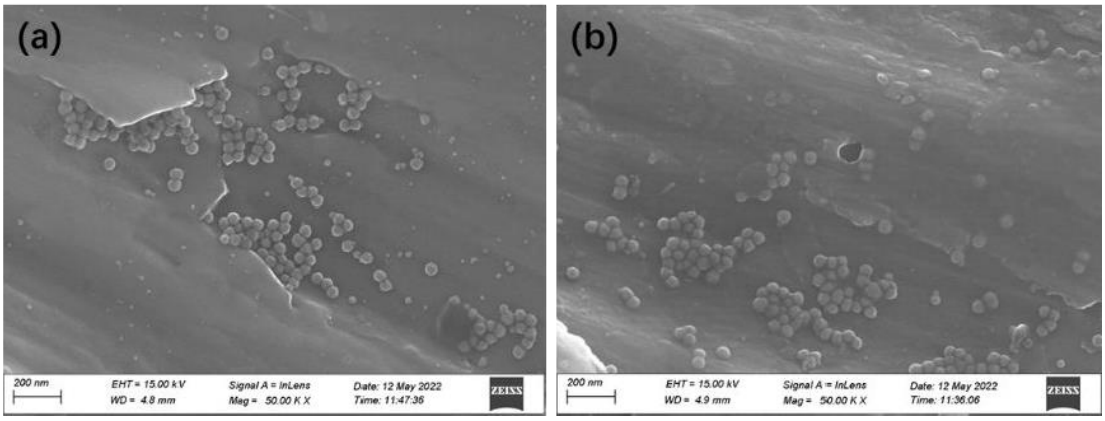

(a) Ti-0.005, (b) Ti-9

Figure 3: Microscopic morphology at the concentration of nanoparticles:

Fig. 3 shows the concentrated areas of nanoparticles in Ti-0.005 and Ti-9. In Ti-0.005, nanoparticles are observed to preferentially grow in defect areas, such as step edges and pits, while in smoother areas, nanoparticles are smaller and less abundant. As the oxidation time increases, the distribution of nanoparticles becomes more random and denser, but remains discontinuous. The same phenomenon has been reported in reference [13].

3.3 Phase composition

The Raman spectra of the oxide films anodized at different times are shown in fig.4(a). Ti-0.005 does not exhibit any characteristic peak of crystalline phases, and contains numerous unstable oxides such as Ti_3O_5 and Ti_2O_3 [14]. A Raman peak at 157 cm^{-1} is observed in Ti-2, but the peak width indicates the formation of anatase TiO_2 with low crystallinity [15], while characteristic peaks of Ti_3O_5 still exist at 263 and 423 cm^{-1}. As the time reaches 5 min, the peaks at 151 ±6, 202 ±4, 400 ±2, 507 ± 5 and 624 ± 10 cm^{-1} are observed due to the increase of anatase TiO_2 content, without other characteristic peaks of oxides, indicating the transformation of unstable intermediate oxides into TiO_2. The intensity of characteristic peak at 151 cm^{-1} increases with prolonged time in stages (II) and (III). Therefore, a longer oxidation time is beneficial for crystallization and an increase in TiO_2 content.

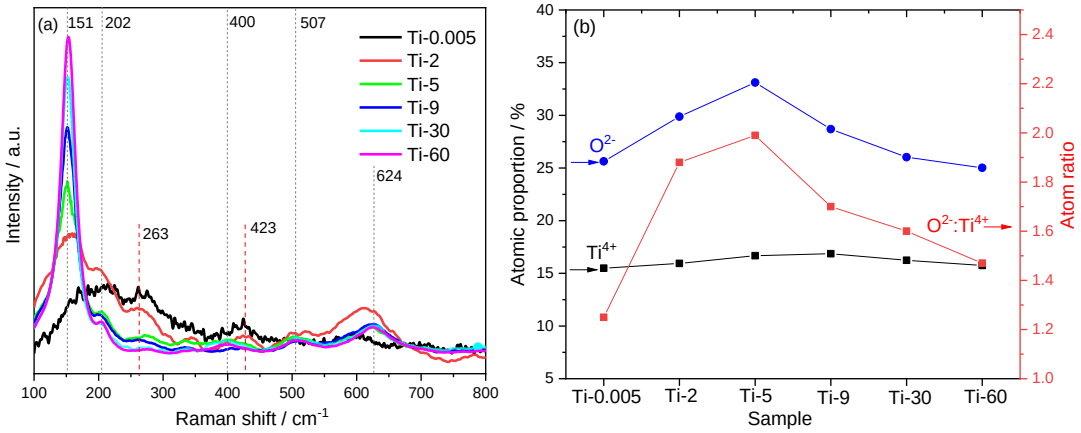

(a) Raman spectra, (b) Changes in Ti^{4+}, O^{2-} composition and O^{2-}/Ti^{4+} ratio

Figure 4: Chemical composition analysis of the oxide films anodized at different times:

The O^{2-}/Ti^{4+} atomic ratio was measured by XPS method, as shown in Fig. 4(b). With the increase of time, the O^{2-}/Ti^{4+} atomic ratio initially increases and then decreases, reaching a maximum value of 2 at 5 min. The high lattice O^{2-} content is beneficial to improve the crystallinity of TiO_2 [12]. The highest concentration of lattice O^{2-} is present in stage (II) and Ti-5 exhibits the highest crystallinity. Previous research has reported that a dense oxide film forms rapidly at the beginning of anodic oxidation with high current density, resulting in well-crystallized oxide film [16-17]. However, our findings suggest that the oxide film is amorphous initially, and the crystallinity of TiO_2 is the highest with fewer crystal defects in stage (II).

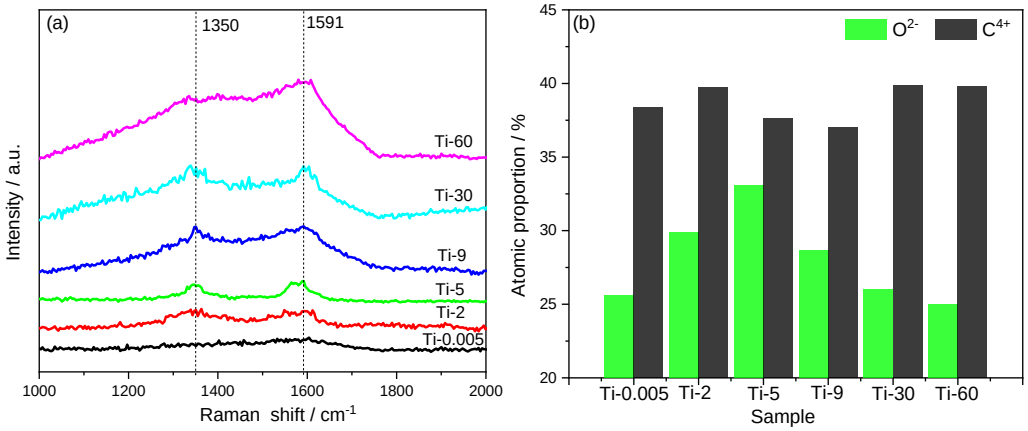

(a) Raman spectra, (b) Changes in C^{4+} and O^{2-} composition

Figure 5: Analysis of C element in oxide films anodized at different times:

To investigate the doping of electrolyte into the oxide film, the Raman spectra of C peak in the range of 0 ~ 4000 cm^{-1} are analyzed, as shown in Fig. 5(a). There are two vibrational modes associated with the rGO structure in the oxide film [18]. The D band at 1350 cm^{-1} and the G band at 1591 cm^{-1} confirm the hybrid structure formed. The binding energy of carbon peak was determined as C 1s by XPS method, and three peaks corresponding to C = C, C-OH and C = O bond were identified. Figure 5(b) analyses the atomic ratios of O^{2-} and C^{4+} at different time. The results shows that C^{4+} is negatively correlated with the changing of O^{2-} content. It is inferred that in stage (I) and (III), rGO in the electrolyte can be successfully doped into the oxide film, and in stage (II), the doped rGO may escape from the oxide film [19].

3.4 Nano-hardness

The load-displacement curves are shown in Fig. 6, while the nano-indentation hardness (*H*) and elastic modulus (*E*) data are presented in Tab. 1. Compared to the substrate, the oxide film exhibits increased *H* and *E*. At 9 min, the hardness peaks at 6.32 GPa, and the elastic modulus peaks at 133.94 GPa. With further extension of oxidation time to 60 min, *H* and *E* of the film decrease. Through the chemical composition analysis of the oxide film, the crystallinity of the oxide film increases gradually during stages (I) and (II), reaching its maximum at stage (II). The change in *H* and *E* follows the same trend as the crystallinity. In stage (III), despite the prolonged time, the crystallinity of the film decreases, leading to increased crystal defects and a gradual decrease of the *H* and *E* after 9 min.

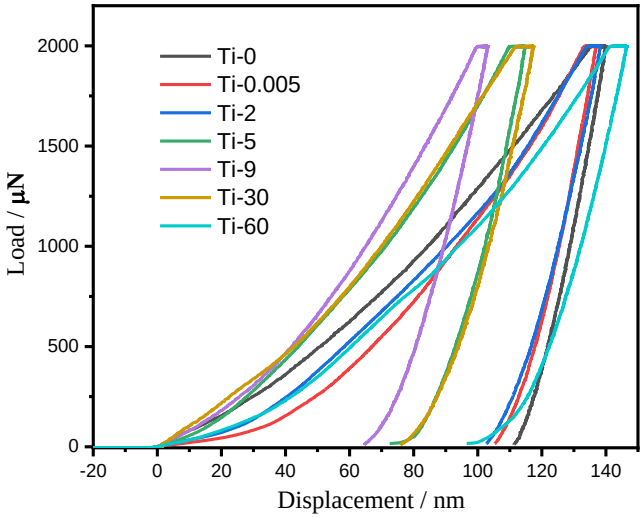

Figure 6: Load-displacement curves of the oxide films anodized at different times

Table 1: Elastic modulus, nano-indentation hardness and fracture toughness indices of oxide films prepared at different times

Sample	E_r (GPa)	H (GPa)	H/E (MPa)	H^3/E^2 (MPa)
Ti-0	111.77	3.29	29.44	2.86
Ti-0.005	110.85	4.15	37.44	5.81
Ti-2	127.36	4.70	36.90	6.39
Ti-5	125.99	5.98	47.46	13.48
Ti-9	133.94	6.32	47.19	14.09
Ti-30	115.04	5.06	43.98	9.78
Ti-60	116.57	4.38	37.57	6.18

The *H*/*E* ratio is a parameter that characterizes the anti-plasticity of oxide films, as shown in Tab. 1. It can be used to study the deformation mechanism of oxide films and predict their wear resistance. The calculated *H*/*E* values of the anodized samples range from 37.44 to 47.46 MPa, which exceed that of the titanium substrate (29.44 MPa) but less than 100 MPa. It indicates that plastic deformation of the oxide film occurs under external forces. The deformation resistance and wear resistance of the oxide film are improved compared with those of the titanium substrate.

3.5 Corrosion resistance

The polarization curves of the samples were measured in a 3.5 wt% NaCl solution. After the test, the corrosion potential (*E*corr) and corrosion current density (*j*corr) were obtained by Tafel extrapolation. The anodic Tafel slope (βa), and cathodic Tafel slope (βc) can be determined by the

extrapolation of straight lines via the Tafel method [20]. The polarization resistance (*R*p) was calculated, and the results are presented in Tab. 2.

Table 2: Results of corrosion resistance of the oxide films prepared at different times

Sample	E_{corr} / MV	β_a / mV dec^{-1}	$-\beta_c$ / mV dec^{-1}	R_p / MΩcm^2	j_{corr} / nA cm^{-2}
Ti-0	-1411	200.03	208.10	0.13	351.9
Ti-0.005	-1116	221.17	186.88	0.30	144.3
Ti-2	-1305	227.26	175.23	0.41	104.5
Ti-5	-1197	237.00	149.04	0.79	50.34
Ti-9	-1189	239.47	168.97	0.63	68.24
Ti-30	-988	237.88	173.76	0.53	82.6
Ti-60	-914	249.65	198.48	0.63	76.5

The *E*corr value reflects the corrosion resistance of the oxide film in a NaCl solution. A higher *E*corr value indicates better stability of the oxide film and lower susceptibility to corrosion. Tab. 2 shows the *E*corr increases with prolonged time, suggesting improved corrosion resistance over time. The polarization curve is divided into cathodic and anodic regions, with βa representing the anodic slope and βc representing the cathodic slope. The calculated βa > βc shows that the electrochemical process of the oxide film is controlled by the cathodic reaction. The cathodic reaction predominates, and the anodic dissolution reaction is inhibited. *J*corr reflects the corrosion rate of the oxide film in NaCl solution. A smaller *J*corr value indicates better stability of the oxide film and lower electrochemical corrosion rate. *J*corr decreased in stage (II) when the time exceeded 5 min. Specifically, Ti-5 exhibited the smallest *J*corr, followed by Ti-9.

4. Conclusions

The pure titanium was anodized at different times in rGO/ C6H8O7 aqueous electrolyte at 50 V. In the initial 2 min, the oxide film is in the growth stage. The film consisted of various non-steady state oxides such as Ti3O5 and Ti2O3. Subsequently, from 2 to 9 min, the oxide film enters the dissolution stage, characterized by a high content of lattice O^{2-}, high crystallinity and low structural defects. The nano-hardness and corrosion resistance of the oxide film in this stage were superior to those of other samples. Finally, from 9 to 60 min, the oxide film continued to grow slowly towards a balanced stage. As time progressed, the thickness of the oxide film slightly increased, while the content of lattice O^{2-} decreased and structural defects increased, leading to a decrease in hardness and corrosion resistance. Therefore, the corrosion resistance and mechanical properties of the oxide films follow a decreasing order of stages (II) > (III) >(I).

Acknowledgement

This work was supported by the National Key Research and Development Program of China (Grant No. 2021YFD1600402), the National Natural Science Foundation (No. 22208263), Shaanxi Provincial Natural Science Basic Research Program (No. 2024JC-YBMS-347), Shaanxi Province Qinchuangyuan "scientist + engineer" team construction project (No. 2024QCY-KXJ-115)

References

[1] M. Shivansh, K. Dova, K.M. Surendra, et al., Oxide growth characteristics, kinetics and mechanism of rutile formation on pure titanium [J]. Vacuum, 2024, 219: 112682.
[2] F.J. Walker, R.A. McKee, High-temperature stability of molecular beam epitaxy-grown multilayer ceramic composites: TiO/Ti_2O_3 [J]. Journal of Crystal Growth, 1992, 116: 235-239.
[3] L.C. Zhang, L.Y. Chen, L.Wang, Surface modification of titanium and titanium alloys: technologies, developments,

and future interests. Advanced Engineering Materials. 2020, 22(5):1901258.
[4] H. Chouirfa, H. Bouloussa, V.U. Migonney, et al., Review of titanium surface modification techniques and coatings for antibacterial applications. Acta biomaterialia. 2019, 83:37-54.
[5] J. Xu, J. Zhang, Y. Shi, et al., Surface modification of biomedical Ti and Ti alloys: a review on current advances. Materials. 2022, 15(5):1749.
[6] M.K. Balbina, O. Agnieszka, Recent advances in electrochemically surface treated titanium and its alloys for biomedical applications: A review of anodic and plasma electrolytic oxidation methods [J]. Materials Today Communications, 2023, 34: 105425.
[7] G. Karan, D.O.M. Ruben, C. Mateusz, et al., Understanding the influence of electrolyte aging in electrochemical anodization of titanium [J]. Advances in Colloid and Interface Science, 2022, 302: 102615.
[8] M. Kaur, K. Singh, Review on titanium and titanium based alloys as biomaterials for orthopaedic applications [J]. Mater. Sci. Eng. C., 2019, 102: 844–862.
[9] W. Juliusz, T. Włodzimierz, P. Mirosława, et al., Titanium anodization in deep eutectic solvents: The effect of anodizing time on the morphology and structure of anodic layers [J]. Applied Surface Science, 2022, 577: 151892.
[10] X. Li, L. Wang, L. Fan, et al., Understanding the effect of fluoride on corrosion behavior of pure titanium in different acids [J]. Corrosion Science, 2021, 192: 109812.
[11] D.R. Barjaktarević, I. Cvijović-Alagić, I. Dimić, et al., Anodization of Ti-based materials for biomedical applications: A review [J]. Metallurgical and Materials Engineering, 2016, 22(3): 129-143.
[12] D. Shan, B.Q. Tao, C.Q. Fang, et al., Anodization of titanium in reduced graphene oxide-citric acid electrolyte [J], Results in Physics, 2021, 24:104060.
[13] C. Chen, C.C. Chen, S.H. Chen, A Review on Production, Characterization, and Photocatalytic Applicationsnof TiO_2 Nanoparticles and Nanotubes [J]. Current Nanoscience 2017, 13(4): 373-393.
[14] A.G. Santos, B.J.A. Moulton, A.A. Cabral, Discoveries about the structure of alkaline earth-bearing borosilicate glasses doped with TiO_2 revealed by Raman spectroscopy [J]. Journal of Non-Crystalline Solids, 2022, 578: 121349.
[15] Y. Chen, J. Chen, J. Liu, et al., Metal-organic framework-derived mixed-phase anatase/rutile TiO_2 towards boosted lithium storage: Surface engineering and design strategy through crystal phase transition[J]. Materials Today Nano, 2022, 20: 100265.
[16] D. Regonini, C.R. Bowen, A. Jaroenworaluck, R. Stevens, A review of growth mechanism, structure and crystallinity of anodized TiO_2 nanotubes, Mater. Sci. Eng., R. 74 (2013) 377-406.
[17] H.Y. Chung, Y.H. Ng, Electrochemical Synthesis of Nanostructured Catalytic Thin Films. Heterogeneous Catalysts: Advanced Design, Characterization and Applications. 2021 Mar 22; 1:39-55.
[18] S. Ebrahimi, A. Bordbar-Khiabani, B. Yarmand, et al., Improving optoelectrical properties of photoactive anatase TiO_2 coating using rGO incorporation during plasma electrolytic oxidation[J]. Ceramics International, 2019, 45(02): 1746-1754.
[19] J. Su, Z. Du, L. Xiao, et al., Graphene oxide coated titanium surfaces with osteoimmunomodulatory role to enhance osteogenesis[J]. Materials Science and Engineering: C, 2020, 113: 110983.
[20] D. Balilas, E. Urbańczyk, M. Sowa, et al., On the electropolishing and anodic oxidation of Ti-15Mo alloy, Electrochim. Acta. 2016, 205: 256-265.